https://doi.org/10.71442/mari2026-0002

ARTICLE

Functionally Reconfigurable Metamaterials Enabled by Tunable Resistors and Diodes

Gaoya Dong[1,2,*], Zhentao Yang[2], Xin He[1] and Xiaolong Yang[1]

[1] School of Computer and Communication Engineering, University of Science and Technology, Beijing, 100083, China
[2] Shunde Innovation School, University of Science and Technology, Beijing, 528399, China

Abstract

This paper presents a functionally reconfigurable metamaterial (FRM) that can satisfy military requirements for electromagnetic communication, radar stealth and high-power electromagnetic shielding. Specifically, the developed FRM is composed of a lossy layer and a frequency selective surface (FSS), which could achieve three different modes by adjusting the tunable resistors and PIN diodes within the FRM. Furthermore, the operating mechanisms of the FRM in these three modes have been analyzed in detail using an equivalent circuit model and transmission line theory. To validate the aforementioned analysis, the FRM was designed and simulated based on these operating mechanisms and professional electromagnetic simulation software. The simulation results demonstrate that the FRM can achieve tri-modal regulation for different polarized electromagnetic waves by adjusting the resistors and PIN diodes. Specifically, it exhibits: the absorption mode is obtained in the 5.92-10.89 GHz range, the transmission mode is achieved in the 7.63-9.22 GHz range, and the reflection mode is realized in the 2.00-9.80 GHz range. Consequently, the designed FRM can be applied in complex military electromagnetic environments.

Keywords: functionally reconfigurable metamaterial, radar stealth, high-power electromagnetic shielding

Submitted: 16 May, 2025
Accepted: 30 July, 2025
Published: 17 December, 2025

Vol. 2026, **No.** 1, 2026.
https://doi.org/10.71442/mari2026-0002

***Corresponding author:**
✉ Gaoya Dong
gaoyadong@ustb.edu.cn

Citation
Gaoya Dong, Zhentao Yang, Xin He and Xiaolong Yang (2026). Functionally Reconfigurable Metamaterials Enabled by Tunable Resistors and Diodes. Mari Papel Y Corrugado, 2026(1), 16–24.

1 Introduction

The artificial electromagnetic metamaterials are composed of meta-units that are arranged either periodically or non-periodically. The configuration and arrangement of these meta-units can be designed to manipulate spatial electromagnetic waves. In military applications, contemporary weapon systems must possess three critical electromagnetic characteristics: namely, reliable electromagnetic communication, reduced radar cross-section, and robust shielding against high-intensity electromagnetic threats. In order to facilitate reliable electromagnetic communication and radar stealth, frequency-selective absorbers (FSRs) featuring a passband and an absorption band have been proposed in references [1-7]. It has been demonstrated that these FSRs possess the capacity to reduce the radar cross section (RCS) of equipment by absorbing electromagnetic waves from the enemy. Furthermore, they have the capability to establish reliable electromagnetic communication within the passband. However, it should be noted that the electromagnetic wave regulation capabilities of FSRs reported in [1-7] were fixed once processing was complete. Thus, the FSRs proposed in [1-7] are inadequate in adapting to the complex and dynamic electromagnetic environments encountered in military scenarios.

In order to obtain dynamic regulation of electromagnetic waves, tunable resistors, capacitors and PIN diodes are utilized in metamaterials to realize tunable absorption [8, 9], transmission [10] and reflection [11] characteristics. In [12-14], the concept of functionally reconfigurable metamaterials

(FRMs) has been proposed on the basis of PIN diodes. The alteration of the PIN diodes enables the generation of a variety of operating modes. Specifically, an FRM based on a four-layer structure incorporating PIN diodes has been proposed in [12], in which the transmission, reflection and electromagnetic focusing modes can be realized by controlling the states of the PIN diodes. The FRM proposed in [14] consists of three layers of split square rings (SSRs) and PIN diodes. It has been demonstrated that this configuration has the capacity to achieve co-polarized reflection and cross-polarized transmission by adjusting the states of the PIN diodes. However, the reconfigurable metamaterials presented in [8-14] are incapable of achieving good electromagnetic communications, radar stealth and high-energy protection through the adjustment of the tunable elements.

To meet military requirements relating to radar stealth, electromagnetic communication and high-power electromagnetic shielding, functionally reconfigurable metamaterials (FRMs) that incorporate absorption, transmission and reflection modes have been developed. In [15], a varactor diode-based FRM has been proposed which possesses these modes. In reflection mode, the reflection coefficient exceeds 0.9 in the 4.40-5.00 GHz range when C_1=2.0pF and C_2=0.4pF . In transmission mode, the transmission coefficient is approximately 0.85 at 4.72 GHz when C_1=2.0pF and C_2=2.2pF . The absorption rate reaches 95.0% at 4.72 GHz in absorption mode when C_1=0.4pF and C_2=1.6pF . Furthermore, an FRM incorporating reflection, transmission and absorption modes was constructed in [16] using varactor and PIN diodes. In transmission mode, the transmission coefficient exceeds -2.9 dB in the 1.68-2.56 GHz range when the PIN diodes on the top and bottom layers are reverse biased. In reflection mode, the reflection coefficient exceeds -1.5 dB in the 2.55-4.62 GHz range when the PIN diodes on the top and bottom layers are forward biased. In absorption mode, the absorption rate is approximately 84% at 1.84-2.85 GHz when the PIN diode on the top layer is reverse biased and the one on the bottom layer is forward biased. Furthermore, the design and optimization efficiency of metamaterials could be effectively improved by adopting reinforcement learning [17-20] and the intelligent singular value decomposition algorithm [21]. It is evident that the FRM structures described in [15, 16] are capable of operating in reflection, transmission, and absorption modes independently. It is noteworthy that the abovementioned FRMs [15, 16] exhibit identical modulation characteristics for both x- and y-polarized electromagnetic waves, thereby lacking the capability to achieve differential regulation for different polarizations.

In this paper, a novel FRM featuring the regulation for different polarized electromagnetic waves in three operating modes has been proposed to satisfy military requirements. The proposed FRM can be mounted on weapons and equipments to achieve reliable electromagnetic communication, radar stealth, and high-power electromagnetic shielding. The presented FRM consists of a lossy layer and an FSS layer, in which tunable resistors and PIN diodes are employed to achieve reflection, transmission, and absorption modes for both x- and y-polarized electromagnetic waves. The operating mechanisms of the designed FRM in its various modes have also been analyzed using lumped element and transmission line theories. Furthermore, these theoretical could provide effective guidance for the design and optimization of the FRM structure. Subsequently, the FRM was simulated and optimized using high-frequency simulation software. The simulation results indicate that the reflection coefficient exceeds -1.9 dB in reflection mode across the 2.00-9.80 GHz frequency range. In transmission mode, the transmission coefficient exceeds -2.0 dB across the 7.63-9.22 GHz range. Furthermore, in absorption mode, the absorption exceeds 80% across the 5.92-10.89 GHz range.

2 The structure of the designed FRM

As illustrated in Figure 1, the meta-unit of the functionally reconfigurable metamaterial (FRM) comprises two vertically stacked functional layers: an upper lossy layer superposed on a lower frequency selective surface (FSS) layer. The lossy layer is constructed by a square ring structure integrated with four lumped resistors and a central square patch. The FSS layer consists of a square ring-shaped slot and four PIN diodes, whose resonant frequency is determined by its dimensions. The specific parameters of the designed FRM are exhibited in Table 1.

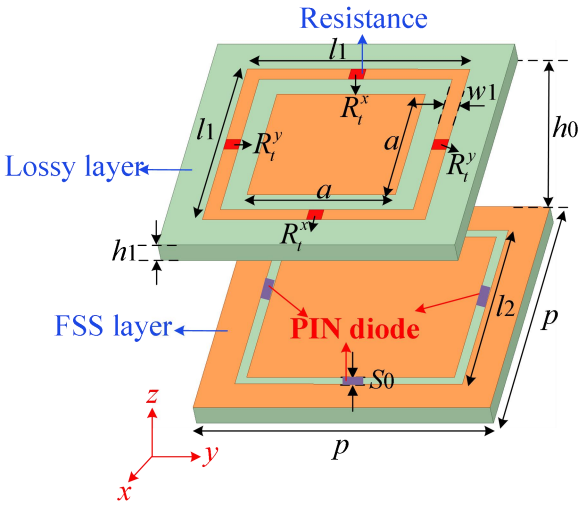

Figure 1. The meta-unit of the designed FRM

Table 1. The detailed parameters of the designed FRM

p	l_1	w_1	a	l_2
12.0 mm	9.0 mm	0.6 mm	12.0 mm	9.2 mm
s_0	h_0	h_1	R_t^x, R_t^y	
0.4 mm	7.5 mm	0.254 mm	0/1000Ω	

3 The Operating Mechanism of the Designed FRM

3.1 Operating mechanism of FRM in "reflection-transmission" mode

The lumped-element equivalent circuit approach was adopted to analyze the operating principles of the proposed FRM. Based on equivalent principles, the equivalent circuit diagram of the designed FRM meta-unit could be derived and exhibited in Figure 2. Specifically, the metallization patterns are equivalent to inductors (L) and capacitors (C), and the air gap between the lossy layer and the FSS layer can be considered equivalent to a transmission line. Furthermore, L_1 in Figure 2 represents a square ring resonator loaded with lumped resistors in the lossy layer, L_2 represents a square metal patch in the lossy layer, and L_3 represents a ring-shaped slot structure in the FSS layer. The wave impedance in free space is denoted by Z_0, the thickness of the air layer is represented by h_0, and R_t is an adjustable resistor, including R_t^x, R_t^x specifically. In addition, the detailed parameters of the lumped-element equivalent circuit for this FRM are exhibited in Table 2.

As shown in Figure 3, when the adjustable resistor value (R_t) is set to 0 Ω, S_21 is below -10.0 dB at 7.63-9.23 GHz. This indicates that electromagnetic waves incident from port 1 cannot be transmitted to port 2 within this frequency range. When R_t is set to 1000 Ω, S_21 is above -2.0 dB at 7.63-9.23 GHz, indicating that electromagnetic waves incident from port 1 can be transmitted to port 2. Consequently, the transmission characteristics of electromagnetic waves can be adjusted by tuning the R_t, and the enhanced transmission performance can be attained with higher values of R_t. Furthermore, the electromagnetic and lumped-equivalent circuit simulation results for this FRM are in good agreement, thereby verifying the correctness of the lumped-equivalent circuit model.

Table 2. The key parameters of lumped equivalent circuit

L_1	C_1	L_2	C_2	L_3
1.87 nH	0.13 pF	0.75 nH	0.05 pF	0.35 nH
C_3	Z_0	h_0	R_t^x, R_t^y	
1.4 pF	377W	7.5 mm	0/1000Ω	

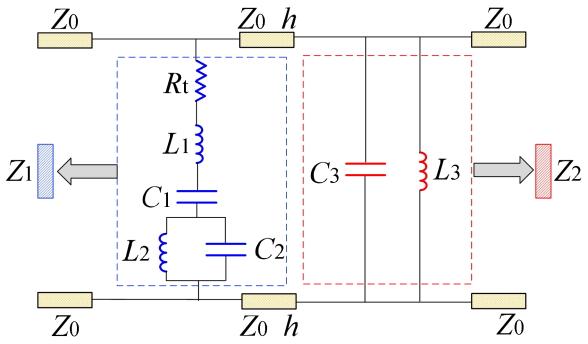

Figure 2. The lumped-equivalent circuit of the FRM unit when the PIN is reverse biased

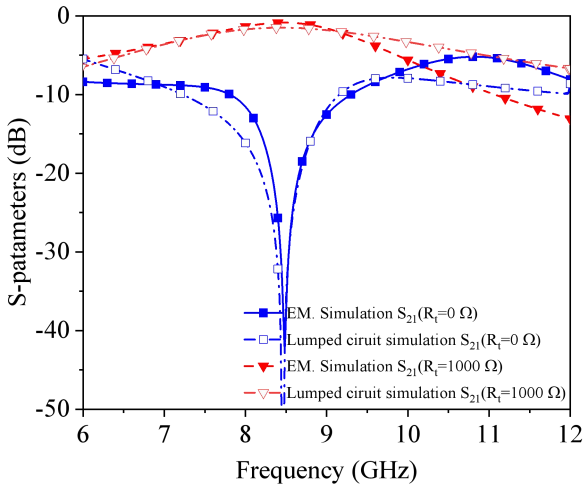

Figure 3. The electromagnetic simulation results and lumped- equivalent circuit simulation results of the FRM

The ABCD transmission matrix for the FRM can be derived based on the lumped-equivalent circuit shown in Figure 2, as given in equation (1). The corresponding scattering parameters can be derived

from this matrix and are presented in equation (2).

$$\begin{bmatrix} A & B \\ C & D \end{bmatrix} = \begin{bmatrix} 1 & 0 \\ 1/Z_1 & 1 \end{bmatrix} \begin{bmatrix} \cos kh & jZ_0 \sin kh \\ j\dfrac{\sin kh}{Z_0} & \cos kh \end{bmatrix} \begin{bmatrix} 1 & 0 \\ 1/Z_2 & 1 \end{bmatrix}$$

$$= \begin{bmatrix} \cos kh + j\dfrac{Z_0}{Z_2}\sin kh & jZ_0 \sin kh \\ \left(\dfrac{1}{Z_1}+\dfrac{1}{Z_2}\right)\cos kh + j\left(\dfrac{1}{Z_0}+\dfrac{Z_0}{Z_1Z_2}\right)\sin kh & \cos kh + j\dfrac{Z_0}{Z_1}\sin kh \end{bmatrix} \quad (1)$$

$$|S_{11}| = \left| \frac{jZ_0(Z_1 - Z_2 - Z_{0\partial}) - Z_0 P \dfrac{1}{\tan\theta}}{(2Q + Z_0 \mathrm{P})\dfrac{1}{\tan\theta} + jZ_0(\mathrm{P} + Z_0)} \right| \quad (2a)$$

$$|S_{21}| = \left| \frac{2Q\dfrac{1}{\sin\theta}}{(2Q + Z_0 \mathrm{P})\dfrac{1}{\tan\theta} + j\left[Z_0(\mathrm{P} + Z_0) + 2\mathrm{Q}\right]} \right| \quad (2b)$$

where: $P = Z_1 + Z_2, Q = Z_1 Z_2, \theta = kh$,

$Z_1 = R_t - j\dfrac{1-\omega^2 L_1 C_1}{\omega C_1} + j\dfrac{\omega L_2}{1-\omega^2 L_2 C_2}$, $Z_2 = j\dfrac{\omega L_3}{1-\omega^2 L_3 C_3}$.

As demonstrated in Figure 2, when Z_1 is selected as 0, the numerator of S_{21} is found to be equal to 0, and the denominator of S_{21} is not equal to 0. Consequently, the designed FRM operates in reflection mode when the Z_1 is assigned to 0. To achieve $Z_1 = 0$, the relevant parameters should satisfy equation (3).

$$R_t = 0 \ \Omega \quad (3a)$$

$$1 - \omega^2 \left(L_1 C_1 + L_2 C_2 + L_2 C_1\right) + \omega^4 L_1 C_1 L_2 C_2 = 0 \quad (3b)$$

Based on (3b), the resonant frequency in the reflection mode was derived and expressed in equation (4).

$$f_r = \frac{1}{2\pi}\sqrt{\frac{q + \sqrt{q^2 - 4p}}{2p}} \quad (4)$$

where: $p = L_1 C_1 L_2 C_2$, $q = L_1 C_1 + L_2 C_2 + L_2 C_1$.

In transmission mode ($S_{11} = 0, S_{21} = 1$), the resonant frequency is determined by the FSS layer, and its expression is given in equation (5). Moreover, the equivalent impedance value of the FSS layer is equivalent to infinity when it is in resonant state. Therefore, it can be concluded that the transmission coefficients expressed in equation (2b) can be simplified as shown in equation (6). As demonstrated in equation (6), S_{21} approaches 1 when R_t is significantly greater than Z_0 (Z_0 =377 W).

$$f_t = \frac{1}{2\pi\sqrt{L_3 C_3}} \quad (5)$$

$$S_{21} = \frac{2}{\left|\dfrac{Z_0}{Z_1} + 2\right|} \quad (6)$$

where: $Z_1 = R_t - j\dfrac{1-\omega^2 L_1 C_1}{\omega C_1} + j\dfrac{\omega L_2}{1-\omega^2 L_2 C_2}$.

3.2 Operating mechanism of FRM in absorption mode

When the diode is forward biased, the FSS layer of the FRM loses its frequency-selective properties and behaves like a solid metal plate. Based on this equivalent circuit principle, the lumped-equivalent circuit of the FRM can be derived and is exhibited in the Figure 4. Subsequently, the lumped-equivalent circuit is employed to analyze the operating mechanism of absorption characteristics in the FRM.

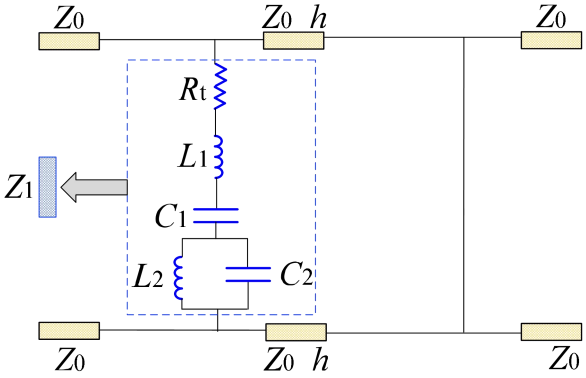

Figure 4. The lumped-equivalent circuit of the designed FRM when the PIN is forward biased.

As observed from Figure 4, the ABCD matrix for the FRM has been derived and is shown in equation (7). The corresponding scattering parameters are derived from equation (7) and presented in equation (8). In addition, the absorption characteristic is determined by the reflection and transmission characteristics, and is expressed in equation (9). It can be concluded from equations (8) and (9) that the absorption characteristics of the FRM are influenced by R_t when the PIN diode is forward biased. The absorption characteristics of the metamaterial can be altered by adjusting the value of R_t .

$$\begin{bmatrix} A & B \\ C & D \end{bmatrix} = \begin{bmatrix} 1 & 0 \\ 1/Z_1 & 1 \end{bmatrix} \begin{bmatrix} \cos kh & jZ_0 \sin kh \\ j\dfrac{\sin kh}{Z_0} & \cos kh \end{bmatrix} = \begin{bmatrix} \cos kh & jZ_0 \sin kh \\ \dfrac{\cos kh}{Z_1} + j\dfrac{\sin kh}{Z_0} & \cos kh + j\dfrac{Z_0}{Z_1}\sin kh \end{bmatrix} \quad (7)$$

where: $Z_1 = R_t - j\dfrac{1-\omega^2 L_1 C_1}{\omega C_1} + j\dfrac{\omega L_2}{1-\omega^2 L_2 C_2} = R_t + jX$,

$X = \dfrac{\omega L_2}{1-\omega^2 L_2 C_2} - \dfrac{1-\omega^2 L_1 C_1}{\omega C_1}$.

$$S_{11} = \frac{Z_0}{2(R_t + jX) + Z_0} \quad (8a)$$

$$S_{21} = \frac{2(R_t + jX)}{(\cos\theta + j\sin\theta)\cdot(2(R_t + jX) + Z_0)} \quad (8b)$$

$$A = 1 - S_{11}^2 - S_{21}^2 \quad (9)$$

4 The Analysis of the Simulated Results

4.1 The analysis in "reflection-transmission" mode

When the PIN diode is reverse biased, the FRM operates in reflection-transmission mode. Figure 5 shows the corresponding reflection and transmission characteristics of the designed FRM with varied R_t^x , R_t^y . As can be seen in Figure 5, the larger resistance values (R_t^x , R_t^y) will result in the poorer reflection performance and the better transmission performance. Specifically, when $R_t^x = R_t^y$ =0 Ω, the reflection coefficients for both x-polarized and y-polarized electromagnetic waves exceed -1.9 dB in the 2.00-9.80 GHz range, indicating that the FRM operates in reflection mode. When $R_t^x = R_t^y$ =1000 Ω, the transmission coefficients for both x-polarized and y-polarized electromagnetic waves exceed -2.0 dB in the 7.63-9.22 GHz range, indicating that the FRM operates in transmission mode. The simulation results in Figure 5 are consistent with the implications of equation (6), thereby further verifying its accuracy.

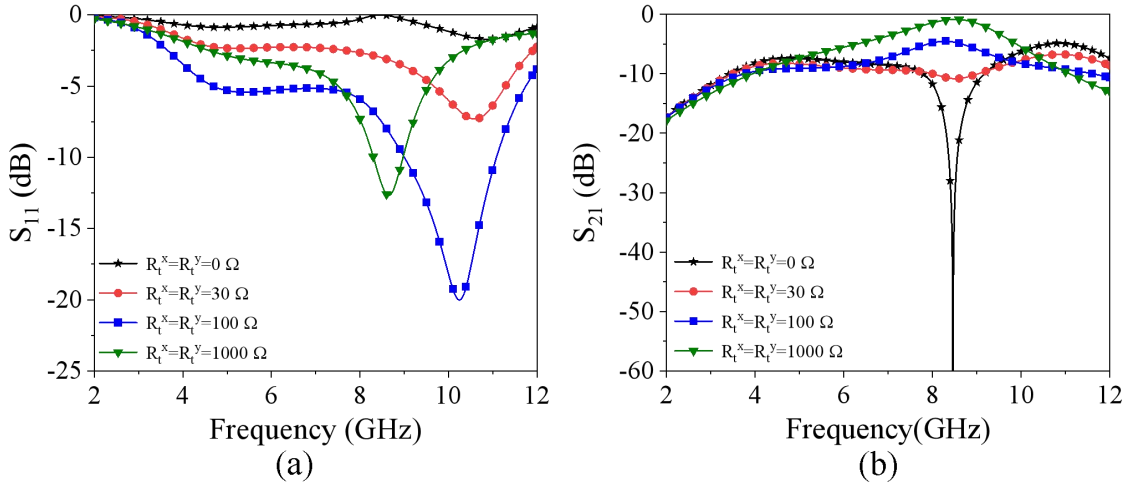

Figure 5. When the PIN diode is reverse biased (a) The reflection and (b) The transmission performances of electromagnetic waves with different R_t^x and R_t^y

Figure 6 shows the reflection and transmission characteristics of the FRM for different polarized electromagnetic waves when the PIN diode is reverse-biased. As observed from Figure 6(a), the reflection coefficient (S_{11}) for x-polarized wave is better than -1.9 dB across the 2.00–9.80 GHz range when R_t^y is set to 1000 Ω and R_t^x to 0 Ω. Meanwhile, the reflection coefficient (S_{11}) for y-polarized wave is not affected by the value of R_t^x when R_t^y =1000 Ω. As can be seen in Figure 6(b), the transmission coefficient (S_{21}) for y-polarized waves exceeds -2.0 dB in the frequency band of 7.63-9.23 GHz when R_t^y is selected as 1000 Ω and R_t^x is selected as 0 Ω, 30 Ω or 100 Ω. This indicates that y-polarized waves can transmit smoothly from port 1 to port 2, regardless of the value of R_t^x . Additionally, Figure 6(b) shows that the transmission coefficient for x-polarized electromagnetic waves (S_{21}^x) can be adjusted by tuning the resistance value of R_t^x . Furthermore, it can also be inferred that the reflection mode for the y-polarized electromagnetic wave can be obtained with R_t^x = 1000 Ω and R_t^y = 0 Ω, while the transmission mode for the x-polarized

electromagnetic wave can be obtained with R_t^x = 1000 Ω and R_t^y = 0, 30 or 100 Ω.

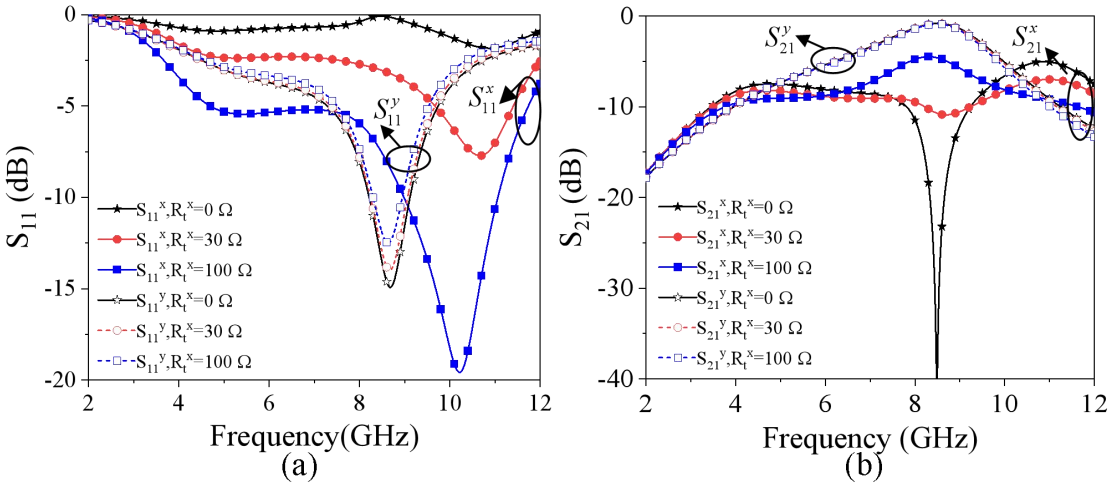

Figure 6. When the PIN diode is reverse biased (R_t^y =1000 Ω) (a) The reflection and (b) The transformation performances of x-polarized electromagnetic wave and y-polarized electromagnetic wave with different resistances (R_t^x)

4.2 The analysis in absorption mode

When the PIN diode is forward biased, the FRM operates in absorption mode. As demonstrated in Figure 7, the designed FRM exhibits different absorption characteristics when subjected to resistance values of 100 Ω, 200 Ω, 500 Ω and 1000 Ω. It can be concluded that the absorption characteristics of the FRM can be adjusted by altering the resistance values (R_t^x). Furthermore, the simulation results agree well with equation (9), as verified by these results.

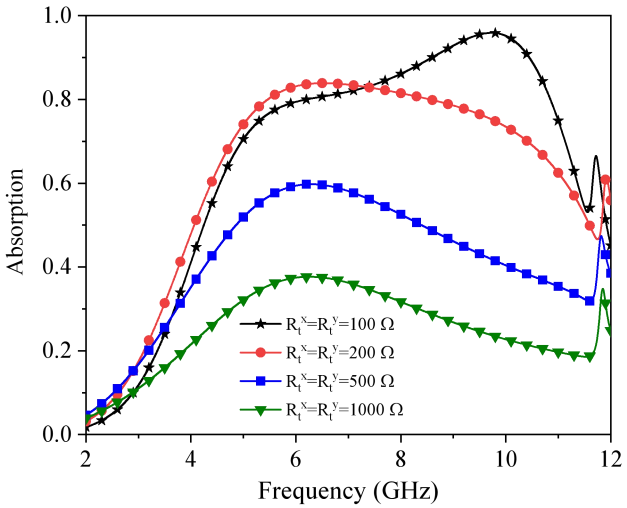

Figure 7. When the PIN diode is forward biased, the absorption characteristics of the FRM with different resistances

When the PIN diode is forward biased, R_t^y is set to 0 and R_t^x is set to 100 Ω, 200 Ω, 500 Ω or 1000 Ω, the absorption characteristics of the FRM for different polarization states are shown in Figure 8. Specifically, for y-polarized waves, when R_t^y = 0, the absorption characteristics are below 0.05 across 2.0-11.5 GHz, indicating negligible absorption. For x-polarized waves in the same band, the absorption characteristics vary with the value of R_t^x. Specifically, the absorption characteristic for an x-polarized wave is greater than 75.0%, ranging from 4.85 GHz to 11.43 GHz.

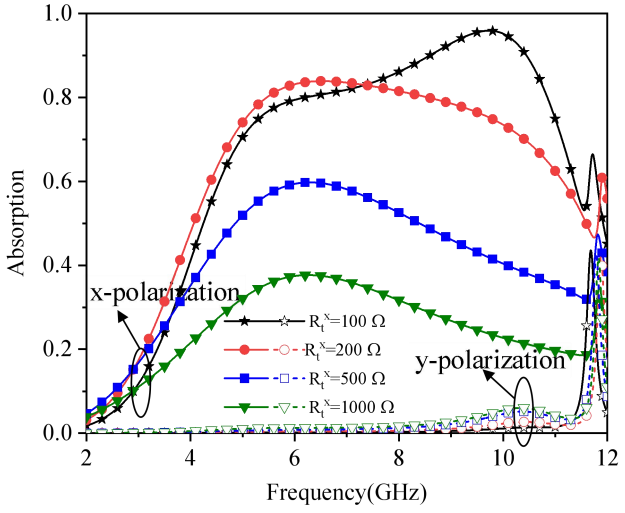

Figure 8. When the PIN diode is forward biased (R_t^y = 0 Ω), (a) The reflection and (b) The transmission characteristics with different resistances (R_t^x)

Above all, the proposed FRM exhibits transmission, reflection, and absorption capabilities for different polarized electromagnetic waves by tuning the resistors and PIN diode states. However, the designed FRM cannot yet be physically fabricated

due to current technological limitations. Specifically, the dimensions and adjustment methods of existing variable resistors do not meet the processing requirements of this FRM. The main performance parameters of the adjustable resistors are presented in Table 3.

Table 3. The main performance parameters of adjustable resistors

Type	*Dimensions(mm^3)*	*Adjustment method*
Potentiometer	9.53×9.53×4.83	manual adjustment
Single-turn potentiometer	3×3×1.5	manual adjustment
Digital Rheostat	3×3×0.8	digital adjustment

Moreover, the design procedure for the FRM is summarized in the following based on the comprehensive analysis presented above.

(1) Determine the design objectives: Determine the absorption rate (A_b), absorption bands (f_{a1}, f_{a2}) in the absorption mode, the transmission coefficient (S_{21}), transmission passband (f_{t1}, f_{t2}) in the transmission mode and the reflection coefficient (S_{11}), reflection bands (f_{r1}, f_{r2}) in the transmission mode. These above parameters will be adopted as the fundamental criteria for evaluating the performance of the FRM.

(2) Design and optimize the lossy layer: Design the lossy layer as illustrated in Figure. 1, which composed of a square ring structure with lumped resistors and a central square patch. When the diode is forward biased, the absorption characteristics (A_b, f_{a1}, f_{a2}) can be optimized by adjusting the resistors (R_t^x , R_t^y). The larger the resistance values (R_t^x , R_t^y), the better the absorption performance. (Figure. 7).

(3) Design and optimize the FSS layer: Design the FSS layer as illustrated in Figure. 1, which composed of a square ring-shaped slot and PIN diodes. When the diode is reverse biased, it operates in the "reflection-transmission" mode. Reflection and transmission characteristics can be optimized by adjusting the resistors (R_t^x , R_t^y). Furthermore, the larger resistance values (R_t^x , R_t^y) will result in the poorer the reflection performance (S_{11}) and the better the transmission performance (S_{21}).

(4) Design and optimize the FRM: Design the FRM by placing the optimized lossy layer on the FSS layer. Reflection, transmission and absorption modes can be achieved by tuning the resistors (R_t) and the forward/reverse biased PIN diodes.

(5) Optimize the regulation for different polarized electromagnetic waves:

(a) $R_t^x \neq R_t^y$ is selected to realize the independent regulation for x-polarized and y-polarized electromagnetic waves.

(b) Optimize the "reflection-transmission" mode: It is observed from Figure. 6 that the FRM operates in "reflection-transmission" mode when the PIN diodes are reverse biased. Adjust the reflection characteristics and transmission characteristics for x-polarized electromagnetic waves (S_{11}^x , S_{21}^x) by adjusting the value of R_t^x when the R_t^y is selected as 1000 Ω. Then, optimize the reflection characteristics and transmission characteristics for y-polarized electromagnetic waves (S_{11}^y , S_{21}^y) by tuning the value of R_t^y when the R_t^x is selected as 1000 Ω.

(c) Optimize the absorption mode: It is observed from Figure.8 that the designed FRM operates in absorption mode when the PIN diodes are forward biased. Optimize the absorption characteristics for x-polarized electromagnetic waves (A_b^x) by adjusting the value of R_t^x when the R_t^y is selected as 0 Ω. Then, adjust the absorption characteristics for y-polarized electromagnetic waves (A_b^y) by tuning the value of R_t^y when the R_t^x is selected as 0 Ω.

(6) Iterate and optimize: Return to step (4) until the designed FRM meets the requirements outlined in step (1), ensuring that the final design satisfies all the desired performance criteria.

5 Conclusion

To adapt the dynamic and complex electromagnetic environments, the FRM is proposed based on the adjustable resistors and PIN diodes. It meets critical military requirements, including radar stealth, electromagnetic communication, and high-power electromagnetic shielding. The proposed FRM integrates a lossy layer and a FSS layer with tunable resistors and PIN diodes, thereby achieving tri-modal functionality. The operating mechanisms of each mode are analyzed using an equivalent circuit model and transmission line theory, thereby providing a clear theoretical foundation for the FRM. The simulation results demonstrate the FRM's consistent performance across various polarizations. Specifically, it achieves stable absorption of hostile

electromagnetic signals within the range of 4.85-11.43 GHz, selective transmissivity for communication bands within the range of 7.63-9.22 GHz, and effective specular reflection against high-energy electromagnetic threats within the range of 2.00–9.80 GHz. These characteristics establish the proposed FRM as a promising candidate for adaptive electromagnetic environment management in military scenarios.

Acknowledgments

This work was supported in part by the Beijing Natural Science Foundation General Project (grant 4232016); the Basic and Applied Basic Research Foundation of Guangdong Province (grant 2022A1515110565); and the National Natural Science Foundation of China (grant 62301027 and grant 62501045).

About the Author

Gaoya Dong received her Ph.D. degree in Electronic Science and Technology from Beijing University of Posts and Telecommunications. She is currently a lecturer in the School of Computer and Communication Engineering, Beijing University of Science and Technology. Her research focuses on filtering antennas, power dividers and functionally reconfigurable metamaterials.

Zhentao Yang received the B.S. degree from Shenzhen University, Shenzhen, China, in 2021. He is currently pursuing the M.S. degree with the School of Computer and Communication Engineering, University of Science and Technology Beijing, Beijing, China. His research interests include electromagnetic metamaterials, machine learning, and algorithm optimization.

Xin He was born in Shandong, China. She graduated from Jining University in 2022 with a B.S. degree in Computer Science and Technology. She received the M.S. degrees in engineering from Qufu Normal University, in 2025. She is currently pursuing the Ph.D. degree in the School of Computer and Communication Engineering, University of Science and Technology Beijing. Her research interests include Fabry-Perot resonant antenna and Multifunctional metasurface.

Xiaolong Yang received his Ph.D. degree in Information and Communication Systems from the University of Electronic Science and Technology, China. He is currently a professor of communication and information systems at the University of Science and Technology in Beijing (100083, China). His research interests include next-generation internet technology, network security and microwave components.

References

[1] Costa F, Monorchio A. A frequency selective radome with wideband absorbing properties[J]. IEEE transactions on antennas and propagation, 2012, 60(6): 2740-2747.

[2] Chen Q, Bai J, Chen L, et al. A miniaturized absorptive frequency selective surface[J]. IEEE antennas and wireless propagation letters, 2014, 14: 80-83.

[3] Ye H, Dai W, Chen X, et al. High-selectivity frequency-selective rasorber based on low-profile bandpass filter[J]. IEEE Antennas and Wireless Propagation Letters, 2020, 20(2): 150-154.

[4] Xia J, Wei J F, Liu Y, et al. Design of a wideband absorption frequency selective rasorber based on double lossy layers [J]. IEEE Transactions on Antennas and Propagation, 2020, 68(7): 5718-5723.

[5] Chen Q, Sang D, Guo M, et al. Frequency-selective rasorber with interabsorption band transparent window and interdigital resonator[J]. IEEE Transactions on Antennas and Propagation, 2018, 66(8): 4105-4114.

[6] Chen Q, Yang S L, Bai J, et al. Design of absorptive/transmissive frequency-selective surface based on parallel resonance [J]. IEEE Transactions on Antennas and Propagation, 2017, 65(9): 4897 -4902.

[7] Sheng X, Gao X, Liu N. Design of frequency selective rasorber with wide transmission/absorption bands[J]. Journal of Physics D: Applied Physics, 2019, 53(9): 09LT01.

[8] Jiang H, Yang W, Li R, et al. A conformal metamaterial-based optically transparent microwave absorber with high angular stability[J]. IEEE antennas and wireless propagation letters, 2021, 20(8): 1399-1403.

[9] Lin Z C, Zhang Y, Li L, et al. Extremely wideband metamaterial absorber using spatial lossy transmission lines and resistively loaded high impedance surface[J]. IEEE Transactions on Microwave Theory and Techniques, 2023, 71(8): 3323-3332.

[10] Boulley L, Goulain P, Laffaille P, et al. Frequency tunable mid-infrared split ring resonators on a phase change material[J]. Photonics and Nanostructures-Fundamentals and Applications, 2024, 61: 101295.

[11] Gao P, Liu H, Xiang C, et al. A new magnetorheological elastomer torsional vibration absorber: structural design and performance test[J]. Mechanical Sciences, 2021, 12(1): 321-332.

[12] Zhang C, Gao J, Cao X, et al. Multifunction tunable metasurface for entire-space electromagnetic wave

manipulation[J]. IEEE Transactions on Antennas and Propagation, 2019, 68(4): 3301-3306.

[13] Li G, Shi H, Yi J, et al. Transmission–reflection-integrated metasurfaces design for simultaneous manipulation of phase and amplitude[J]. IEEE Transactions on Antennas and Propagation, 2022, 70(7): 6072-6077.

[14] Liu X, Li S, Yang H, et al. Transmission-Reflection Multifunctional 2-Bit Coding Metasurface with Multiple Beams[C]//2023 IEEE MTT-S International Microwave Workshop Series on Advanced Materials and Processes for RF and THz Applications (IMWS-AMP). IEEE, 2023: 1-3.

[15] Song X, Zhu W. Reconfigurable Metasurface for Dynamical Modulation of Reflection, Transmission, and Absorption[C]//2021 IEEE International Symposium on Antennas and Propagation and USNC-URSI Radio Science Meeting (APS/URSI). IEEE, 2021: 1221-1222.

[16] Sainadh P M, Ghosh S. A Reconfigurable Frequency Selective Surface Switching between Absorption, Transmission, and Reflection, along with Frequency Tunability[C]//2023 IEEE Microwaves, Antennas, and Propagation Conference (MAPCON). IEEE, 2023: 1-5.

[17] Hu S, Li M, Xu J, et al. Electromagnetic metamaterial agent[J]. Light: Science & Applications, 2025, 14(1): 12.

[18] Rosafalco L, De Ponti J M, Iorio L, et al. Optimised graded metamaterials for mechanical energy confinement and amplification via reinforcement learning[J]. European Journal of Mechanics-A/Solids, 2023, 99: 104947.

[19] Liu H, Huang W, Kim D I, et al. Towards efficient task offloading with dependency guarantees in vehicular edge networks through distributed deep reinforcement learning[J]. IEEE Transactions on Vehicular Technology, 2024, 73(9): 13665-13681.

[20] Liu H, Li T, Jiang F, et al. Coverage optimization for large-scale mobile networks with digital twin and multi-agent reinforcement learning[J]. IEEE Transactions on Wireless Communications, 2024.

[21] Lv W, Liu C, Liu H, et al. Millimeter wave radar for short-term heart rate measurement using intelligent singular value decomposition noise reduction algorithm[J]. IEEE Transactions on Instrumentation and Measurement, 2024.